Research in Astron. Astrophys. **2009** Vol. **9** No. **11**, 1215–1229
*http://www.raa-journal.org* *http://www.iop.org/journals/raa*

***R**esearch in*
***A**stronomy and*
***A**strophysics*

# Stellar ages and metallicities of nearby elliptical galaxies *

Bai-Tian Tang, Qiu-Sheng Gu and Song Huang

Department of Astronomy, Nanjing University, Nanjing 210093, China; *tangbaitian@gmail.com; qsgu@nju.edu.cn*

Received 2009 March 16; accepted 2009 July 12

**Abstract** Stellar ages and metallicities are crucial for understanding the formation and evolution of elliptical galaxies. However, due to the age−metallicity degeneracy, it is hard to measure these two parameters accurately with broad-band photometry. In this paper, we observed high-resolution spectra for a sample of 20 nearby elliptical galaxies (EGs) with the NAOC 2.16 m telescope, and determined stellar ages and metallicities by using the empirical population synthesis and Lick/IDS index system methods. We found that stellar ages from these two methods are consistent with each other for purely old EGs; however, stellar metallicities show a zeropoint offset of 0.5 $Z_{\odot}$. Our results confirm that stellar populations in low-density environment galaxies are more diverse compared to their high-density counterparts. We also investigated the element abundance−galaxy mass relation for nearby elliptical galaxies.

**Key words:** galaxies: elliptical and lenticular, cD — galaxies: statistics — galaxies: stellar content

## 1 INTRODUCTION

Recent observations with modern space facilities, like the *Hubble* and *Spitzer Space Telescopes*, suggest that elliptical galaxies (EGs) are more complicated than a simple system consisting of an old stellar population. Properties of EGs, like stellar properties, central surface brightness distributions, black hole activity, and the distributions and origins of interstellar media, are now being hotly debated. Many studies have reported that cool interstellar media (dust and molecular gas) have been detected in EGs (Knapp et al. 1989; Temi et al. 2004; Kaneda et al. 2005). Kaneda et al. (2008) even detected polycyclic aromatic hydrocarbons (PAHs) in 14 dusty EGs. Most recently, Huang & Gu (2009) reported 13 star-forming elliptical galaxies by using the Sloan Digital Sky Survey spectroscopic database. Thus, it is necessary to study nearby EGs in more detail.

Stellar ages and metallicities of EGs have recorded the star formation and chemical history since galaxy formation, so they are powerful parameters for recovering the formation and evolution history of EGs. For resolved clusters, stellar ages and metallicities can be determined by a color−magnitude diagram (CMD) (Zorotovic et al. 2009). However, this does not work for unresolved systems like EGs. Even worse, due to the age−metallicity degeneracy ($\delta \log(\mathrm{Age})/\delta \log(Z) = -3/2$, Worthey 1994), it is hard to determine the stellar age and metallicity from the broad-band optical colors.

Nowadays, there are two main methods available for separately estimating the stellar age and metallicity. One is to disentangle the age−metallicity degeneracy by employing the metal absorption line indices (Burstein et al. 1984; Faber et al. 1985; Worthey 1994). The Lick/IDS index system

* Supported by the National Natural Science Foundation of China.

(Worthey 1994; Worthey & Ottaviani 1997) studied the stellar age and chemical element abundance by using a series of stellar absorption lines, such as H$\beta$, H$\gamma$, Mgb, and Fe 5270. By measuring the Lick indices and then combining them with the stellar population model (Worthey 1994; Bruzual & Charlot 2003 (BC03); Thomas et al. 2003 (TMB03); Schiavon 2007 (S07)), the stellar age and metallicity can be determined. Graves et al. (2008) compiled a specific code, EZ_Ages [1], which chose the S07 stellar population model, and utilized the "Sequential Grid Inversion Algorithm" for the SDSS spectrum. EZ_Ages can estimate not only the stellar age and [Fe/H], but also the abundances of other chemical elements, which depend on the sensitivities of Lick indices to abundance variations (Korn et al. 2005; Serven et al. 2005).

On the other hand, Bica (1988) proposed the empirical population synthesis method, which derived the stellar age and metallicity by comparing the observed spectra with the linear combination of a set from a single stellar population with different stellar ages and metallicities. Accompanied by more effective calculations (Cid Fernandes et al. 2001), higher-resolution spectra and finer stellar population models (BC03; TMB03), the empirical population synthesis method is entering a new epoch. Based on the single stellar population model from BC03, Cid Fernandes et al. (2004) compiled the empirical population synthesis analysis program, *Starlight* [2].

However, the BC03 model does not consider the $\alpha$ element enhancement, which is ubiquitous in EGs (Trager et al. 2000a,b; TMB03). On the other hand, the "Sequential Grid Inversion Algorithm" in EZ_Ages cannot deal with the complexity that Lick indices are outside of the model grids. Moreover, the age indicator, H$\beta$, may be contaminated by young stellar populations (Burstein et al. 1984; Worthey 1996a). In this paper, based on relatively high spectral resolution optical spectra and the theoretical model of TMB03, we applied a probability density method (Annibali et al. 2007) to a sample of 20 nearby EGs in order to derive their stellar ages and metallicities, and compared our results with the above two methods.

This paper is organized as follows: sample selection and data reduction are described in Section 2; the basic results of the observations are presented in Section 3; the results are discussed in Section 4; and conclusions are given in Section 5.

## 2 OBSERVATIONS AND SPECTRAL EXTRACTIONS

The EGs in our sample are selected from the Palomar optical spectroscopic survey (Ho et al. 1995; 1997), which includes all nearby galaxies satisfying $B_T < 12.5$ mag in the northern hemisphere. This sample is statistically complete and contains both active and inactive EGs. However, the optical spectra available in Ho et al. (1995) are discrete in two parts: the blue section covers $\sim 4230 - 5100$ Å, with spectral resolution FWHM $\sim 4$ Å; the red one covers $\sim 6210 - 6860$ Å, with spectral resolution FWHM $\sim 2.5$ Å. Since the main purpose of their work is to recover weak nuclear activity, their spectra miss some important absorption lines for constraining stellar properties, such as the 4000 Å break, Mgb5175, Fe 5270, etc. Therefore, we picked out all EGs, and re-observed and obtained the spectra with the 2.16 m telescope of NAOC; a 600 lines mm$^{-1}$ grating was used. The spectral resolution is 2.4 Å, covering 3800 Å to 6200 Å. In this paper, we present 20 EGs, 13 of which are active EGs (LINERS & transition objects) and 7 are inactive ones. More details are listed in Table 1.

The images were reduced with the standard procedures in the IRAF package. The spectrum of the central 2.5 arcsec region was extracted with *doslit* in IRAF. In all cases, the spectra were bias-corrected, and divided by a normalized flat field image in order to remove the pixel-to-pixel variations. Cosmic rays were replaced by an average of their neighboring pixels. The wavelength calibration was accomplished with the Fe-He-Ar arc spectrum and a third-order spline3 function was typically fitted to over 20 comparison lines and the RMS is lower than 0.4 Å. All spectra were flux-calibrated with standard stars (e.g., Hiltner600, Feige34, Feige56, and BD+26 2606). Finally, we shifted the spectra to the rest-frame. Figure 1 shows an example of the reduced spectrum of NGC 3377.

[1] *http://www.ucolick.org/∼ graves/ez_ages.html*

[2] *http://www.starlight.ufsc.br/*

**Table 1** Observations and Global Properties

| Name | Obs Date | Exp Time (s) | S/N | $B_T$ (mag) | D (Mpc) | $M_{B_T^0}$ (mag) | Class |
|---|---|---|---|---|---|---|---|
| (1) | (2) | (3) | (4) | (5) | (6) | (7) | (8) |
| NGC 2768 | 2008–02–26 | 3600 | 26.5 | 10.84 | 23.7 | –21.17 | L2 |
| NGC 2832 | 2008–02–28 | 2700 | 36.2 | 12.87 | 91.6 | –22.24 | L2 |
| NGC 3193 | 2008–02–27 | 3600 | 31.4 | 11.83 | 23.2 | –20.10 | L2 |
| NGC 3226 | 2008–02–28 | 3600 | 33.8 | 12.30 | 23.4 | –19.40 | L1.9 |
| NGC 3377 | 2008–02–27 | 2700 | 28.1 | 11.24 | 8.1 | –18.47 | A |
| NGC 3379 | 2008–02–26 | 3600 | 37.2 | 10.24 | 8.1 | –19.36 | L2/T2 |
| NGC 3608 | 2008–02–28 | 3600 | 32.4 | 11.70 | 23.4 | –20.16 | L2/S2 |
| NGC 3610 | 2008–04–12 | 3600 | 35.3 | 11.70 | 29.2 | –20.79 | A |
| NGC 3640 | 2008–04–13 | 3600 | 33.0 | 11.36 | 24.2 | –20.73 | A |
| NGC 4125 | 2008–02–26 | 2700 | 38.1 | 10.65 | 24.2 | –21.25 | T2 |
| NGC 4278 | 2008–02–27 | 2700 | 39.7 | 11.09 | 9.7 | –19.38 | L1.9 |
| NGC 4365 | 2008–02–28 | 2700 | 38.5 | 10.52 | 16.8 | –20.64 | A |
| NGC 4406 | 2008–04–13 | 3600 | 36.2 | 9.83 | 16.8 | –21.39 | A |
| NGC 4486 | 2008–04–13 | 3600 | 43.2 | 9.59 | 16.8 | –21.64 | L2 |
| NGC 4552 | 2008–04–12 | 3600 | 37.1 | 10.73 | 16.8 | –20.56 | T2 |
| NGC 4621 | 2008–02–28 | 2700 | 33.9 | 10.57 | 16.8 | –20.64 | A |
| NGC 4636 | 2008–02–27 | 2700 | 35.7 | 10.43 | 17.0 | –20.72 | L1.9 |
| NGC 4649 | 2008–02–26 | 2700 | 45.7 | 9.81 | 16.8 | –21.43 | A |
| NGC 5813 | 2008–04–12 | 3600 | 32.3 | 11.45 | 28.5 | –20.85 | L2 |
| NGC 5846 | 2008–04–13 | 3600 | 31.6 | 11.05 | 28.5 | –21.36 | T2 |

Notes: Col. (4): S/N in the spectral range of $4730 - 4780$Å.
Col. (5): Apparent $B$ magnitude.
Col. (6): Distance.
Col. (7): Extinction corrected absolute $B$ magnitude.
Col. (8): Nuclear spectral type from the Palomar survey (Ho et al. 1997): L = LINER; T = Transition object; A = absorption-line nuclei (inactive).

## 3 ANALYSIS METHODS

### 3.1 Starlight

The empirical population synthesis program, 'Starlight' (Cid Fernandes et al. 2004; Gu et al. 2006), linearly combined 45 simple stellar populations (SSPs) (15 ages and 3 metallicities) from BC03 to find the best fitting of the observed spectrum ($O_\lambda$). The synthesis spectrum is given by Cid Fernandes et al. (2004):

$$M_\lambda = M_{\lambda_0}\Big(\sum_{i=1}^{N} x_i b_{i,\lambda} r_\lambda\Big) \otimes G(v,\sigma), \tag{1}$$

$M_{\lambda_0}$ is the synthesized flux at normalized wavelength $\lambda_0$, $x_i$ is the contribution of the $i$th SSP to the synthesized flux at $\lambda_0$, $b_{i,\lambda}$ is the spectrum of the $i$th SSP normalized at $\lambda_0$, and $r_\lambda \equiv 10^{-0.4(A_\lambda - A_{\lambda_0})}$ represents the reddening term. $G(v,\sigma)$ is the line-of-sight stellar motions which are modeled by Gaussian distributions centered at velocity ($v$) and with dispersion ($\sigma$), and $\otimes$ denotes the convolution operator. Extinction in 'Starlight' is parameterized by $A_V$, utilizing the Galactic extinction law of Cardelli et al. (1989) with $R_V = 3.1$. In particular, the strong emission lines, like H$\beta$, [OIII]4959, 5007, are masked during the fitting to avoid probable contamination. The similarity between the synthesized and observed spectra is weighted by $\chi^2 = \sum_\lambda [(O_\lambda - M_\lambda) w_\lambda]^2$, where $w_\lambda^{-1}$ is the error in $O_\lambda$. More details are given in Cid Fernandes et al. (2004). Figure 1 illustrates the spectral synthesis results of NGC 3377.

After finding the best fitting synthesized spectrum, we derive the flux-weighted age and metallicity as (Cid Fernandes et al. 2004):

$$\langle \log t_* \rangle_L = \sum_{i=1}^{45} x_i \log t_i; \qquad \langle \log Z_* \rangle_L = \sum_{i=1}^{45} x_i \log Z_i\,, \tag{2}$$

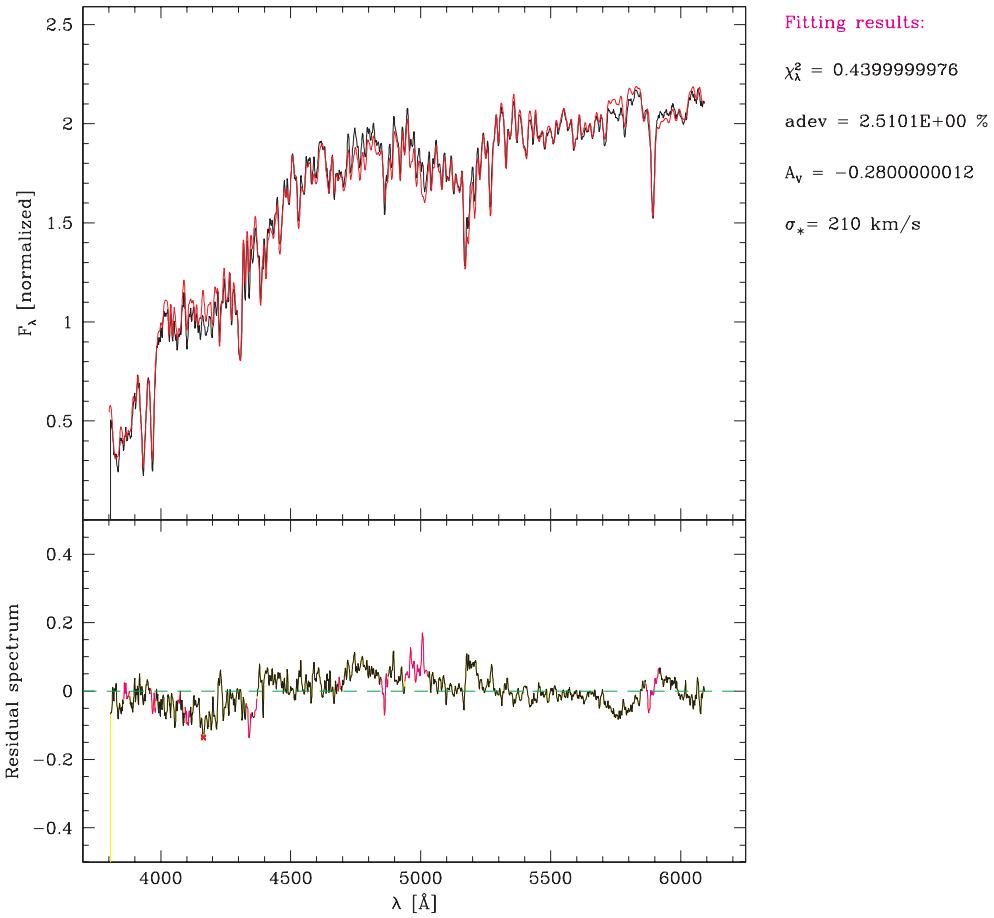


**Fig. 1** Spectral population synthesis results of NGC 3377. *Top*: Observed (*black*) and model (*red*) spectra. *Bottom*: Residual spectrum, with masked regions in pink (see electronic version).

where $t_i$ and $Z_i$ denote the age and metallicity of the $i$th SSP, respectively. The results are presented in Table 2.

### 3.2 EZ_Ages

Graves & Schiavon (2008) compiled the program, EZ_Ages, which determined the stellar age and element abundances by using the Lick/IDS index system. The results indicated that various Lick indices are sensitive to only a few element abundances (Korn et al. 2005; Serven et al. 2005), where H$\beta$ and $\langle$Fe$\rangle$ (the average of Fe 5270 and Fe 5335) are the most representative ones. EZ_Ages measures the two Lick indices, H$\beta$ and $\langle$Fe$\rangle$, then determines the age and [Fe/H] inversely from the S07 stellar population model, which consists of a solar-scaled isochrone and an $\alpha$-enhanced isochrone ($[\alpha/\mathrm{Fe}] = +0.42$). The "Sequential Grid Inversion Algorithm" is applied for this purpose. The algorithm divides the loose model grid-boxes (23 model ages times 4 possible values of [Fe/H]) into closer ones (1000 $\times$ 1000 for each model grid-box in EZ_Ages), assuming that age and [Fe/H] change linearly in each grid-box. By using this algorithm, the data point in the H$\beta$-$\langle$Fe$\rangle$ space is converted into age and [Fe/H]. If the measured H$\beta$ or $\langle$Fe$\rangle$ lie outside of the model grids, EZ_Ages returns a "NAN." Meanwhile, Graves &

**Table 2** Stellar Ages and Metallicities

| Gal Name | $\mathrm{Age_{SL}}$ (Gyr) | $\mathrm{Age_{EZ}}$ (Gyr) | $\mathrm{Age_{PD}}$ (Gyr) | $\mathrm{Age_{PD2}}$ (Gyr) | $Z_{\mathrm{SL}}$ ($Z_{\odot}$) | $Z_{\mathrm{EZ}}$ ($Z_{\odot}$) | $Z_{\mathrm{PD}}$ ($Z_{\odot}$) | $Z_{\mathrm{PD2}}$ ($Z_{\odot}$) |
|---|---|---|---|---|---|---|---|---|
| (1) | (2) | (3) | (4) | (5) | (6) | (7) | (8) | (9) |
| NGC 2768 | 12.21 | 13.94 | 10.07 | 10.46 | 1.38 | 1.25 | 2.24 | 2.24 |
| NGC 2832 | 10.62 | 5.66 | 8.18 | 9.66 | 2.05 | 2.90 | 2.67 | 2.83 |
| NGC 3193 | 10.49 | 10.52 | 8.25 | 9.36 | 1.49 | 1.32 | 2.01 | 1.93 |
| NGC 3226 | 9.13 | NAN | 7.20 | 7.54 | 1.55 | NAN | 1.49 | 1.58 |
| NGC 3377 | 13.0 | 3.44 | 3.47 | 10.00 | 1.71 | 1.80 | 2.24 | 1.00 |
| NGC 3379 | 13.0 | 9.76 | 8.51 | 10.03 | 1.75 | 1.54 | 2.24 | 2.24 |
| NGC 3608 | 11.28 | 10.17 | 9.68 | 9.56 | 1.63 | 2.74 | 2.72 | 2.93 |
| NGC 3610 | 8.64 | 2.33 | 2.00 | 3.77 | 1.24 | 1.98 | 2.24 | 2.12 |
| NGC 3640 | 12.94 | 3.63 | 3.49 | 9.86 | 1.28 | 1.96 | 2.68 | 1.50 |
| NGC 4125 | 12.99 | NAN | 9.86 | 9.62 | 1.43 | NAN | 1.84 | 2.06 |
| NGC 4278 | 13.0 | NAN | 7.18 | 7.94 | 2.33 | NAN | 1.57 | 1.67 |
| NGC 4365 | 7.7 | 6.94 | 8.36 | 8.80 | 2.00 | 2.50 | 2.86 | 2.69 |
| NGC 4406 | 13.00 | 10.17 | 11.09 | 9.89 | 2.50 | 1.95 | 2.24 | 2.51 |
| NGC 4486 | 6.59 | NAN | 7.02 | 7.29 | 1.67 | NAN | 0.97 | 1.54 |
| NGC 4552 | 13.0 | 12.64 | 11.59 | 10.48 | 2.00 | 1.42 | 2.24 | 2.24 |
| NGC 4621 | 11.69 | 9.39 | 11.57 | 10.97 | 1.84 | 1.97 | 2.24 | 2.24 |
| NGC 4636 | 13.0 | NAN | 8.33 | 8.58 | 2.50 | NAN | 3.51 | 3.12 |
| NGC 4649 | 13.0 | 6.63 | 7.72 | 9.39 | 2.50 | 2.71 | 3.24 | 2.99 |
| NGC 5813 | 12.98 | 14.51 | 9.61 | 11.03 | 1.41 | 1.15 | 2.24 | 2.24 |
| NGC 5846 | 12.16 | NAN | 10.10 | 11.11 | 2.19 | NAN | 2.05 | 2.24 |

Notes: SL for Starlight, EZ for EZ_Age, PD for the probability density method using $\mathrm{H}\beta$ as the age indicator, PD2 for the probability density method using $\mathrm{H}\gamma_{\mathrm{F}}$ as the age indicator. The metallicity computed by EZ_Ages is obtained through equation $[\mathrm{Z/H}] = [\mathrm{Fe/H}] + 0.94[\mathrm{Mg/Fe}]$ mentioned in TMB03. "NAN" represents the galaxies that were not computed in EZ_Ages. In this case, the stellar age will be set at a maximum value of (15 Gyr)— all the data points of these galaxies exceed the model grids in the older population direction; the stellar metallicity will be set to zero and excluded in the comparison.

Schiavon (2008) compared the results of EZ_Ages with Thomas et al. (2005) (TMB05), and derived a consistent result. We applied EZ_Ages to our sample EGs. The results are given in Table 2.

### 3.3 Probability Density Method

By utilizing the probability density method (Annibali et al. 2007), we can calculate the probability density of Lick indices to each model grid (in this paper, we adopt the TMB03 model), and determine the probability density weighted stellar age and metallicity. Detailed steps are presented as follows:

1. Broadening the observed spectrum to match the Lick/IDS System.
   The resolution of the Lick/IDS system is between $\sim 7 - 10$ Å depending on different wavelengths (Trager et al. 1998), while the resolution of our observation is 2.4 Å. Therefore, in order to resemble the general properties of the original spectra obtained by the Lick group, we convolve the observed spectra by a Gaussian distribution with velocity dispersion $\sigma_{\mathrm{smooth}}(\lambda)$ (Kuntschner 2000):

$$\sigma^2_{\mathrm{smooth}}(\lambda) = \frac{\sigma^2_{\mathrm{Lick}}(\lambda) - \sigma^2_{\mathrm{obs}}(\lambda)}{8\ln 2}, \tag{3}$$

   where $\sigma_{\mathrm{Lick}}(\lambda)$ and $\sigma_{\mathrm{obs}}(\lambda)$ represent the resolutions of the Lick/IDS system and our observation, respectively. We would like to thank Haralad Kuntschner for providing us with the main program to down-grade our spectral resolution.
2. Measuring the Lick Indices and errors.

The Lick/IDS index system defines 25 indices with a central bandpass and a pseudocontinuum bandpass (Worthey 1994; Worthey & Ottaviani 1997). For the atomic index:

$$\mathrm{EW} = \int_{\lambda_1}^{\lambda_2} \Big(1 - \frac{F_{I\lambda}}{F_{C\lambda}}\Big) d\lambda. \tag{4}$$

For the molecular index:

$$\mathrm{Mag} = -2.5 \log \Big[ \Big( \frac{1}{\lambda_2 - \lambda_1} \Big) \int_{\lambda_1}^{\lambda_2} \frac{F_{I\lambda}}{F_{C\lambda}} d\lambda \Big], \tag{5}$$

where $F_{I\lambda}$ and $F_{C\lambda}$ represent the fluxes per unit wavelength in the central bandpass and the continuum flux in the central bandpass, respectively.
For error estimation, we adopt the method in Cardiel et al. (1998):

$$\sigma^2[j] = \frac{1}{g} N_c[j] + \sigma^2_{\mathrm{RN}}[j], \tag{6}$$

where $\sigma[j]$ is the variance in pixel$[j]$, $g$ is the gain of the A/D converter, $N_{\mathrm{c}}[j]$ is the number of counts in pixel$[j]$, and $\sigma_{\mathrm{RN}}[j]$ is the read-out noise.
$LECTOR$[3] is a Fortran program which measures indices and estimates errors. After inputting the spectra and some parameters (gain of A/D converter, read-out noise), $LECTOR$ will expediently measure the indices and errors.

3. Correcting the effect of velocity dispersion.
The stellar velocity dispersion tends to broaden the spectral features, and reduce the observed absorption line indices. In order to compare with the raw indices of the stellar population model, we need to calibrate the indices without velocity dispersion. We adopt the correction method mentioned in Kuntschner (2004).
For the atomic index:

$$I_j^{\mathrm{corr}} = I_j^{\mathrm{raw}} \times (1.0 + \sum_{i=1}^{3} a_{i,j} \sigma^i). \tag{7}$$

For the molecular index:

$$I_j^{\mathrm{corr}} = I_j^{\mathrm{raw}} + \sum_{i=1}^{3} a_{i,j} \sigma^i, \tag{8}$$

where $I_j^{\mathrm{raw}}$ and $I_j^{\mathrm{corr}}$ represent the index before and after the correction, respectively, $a_{i,j}$ is the correction coefficient given by Kuntschner (2004), and $\sigma$ is the velocity dispersion estimated by 'Starlight'.

4. Determining Age and Metallicity.
By matching the observed Lick indices with the stellar population model, we can determine the stellar age and metallicity. As far as we know, two methods can work here: interpolation and the probability density method. The former one is applied in EZ_Ages, but the disadvantage is that it cannot estimate the age and metallicity if Lick indices are outside of the model grids. Thus, referring to the probability density method in Annibali et al. (2007), we derive the stellar ages and metallicities of our galaxy sample.
First, we choose three Lick indices, and compare the observed values with the stellar population model. In order to disentangle the age−metallicity degeneracy more efficiently, (H$\beta$, $\langle$Fe$\rangle$, Mgb), (H$\gamma$, $\langle$Fe$\rangle$, Mgb), (H$\delta$, $\langle$Fe$\rangle$, Mgb) are usually adopted. We call $(x_0, y_0, z_0)$ the observed indices and $(\sigma_x, \sigma_y, \sigma_z)$ the associated errors. For each point $(t, Z, \alpha)$ in the (age, metallicity, [$\alpha$/Fe]) space (G

[3] *http://www.iac.es/galeria/vazdekis/*

space), the probability density of $(x_{(t,Z,\alpha)}, y_{(t,Z,\alpha)}, z_{(t,Z,\alpha)})$ in the stellar population model is the solution to the observed indices, which is defined as (assuming errors have a Gaussian distribution):

$$P_{t,Z,\alpha} = \frac{1}{\sqrt{(2\pi)^3}\sigma_x\sigma_y\sigma_z} \exp\Big[-\frac{1}{2}\Big(\frac{x-x_0}{\sigma_x}\Big)^2 - \frac{1}{2}\Big(\frac{y-y_0}{\sigma_y}\Big)^2 - \frac{1}{2}\Big(\frac{z-z_0}{\sigma_z}\Big)^2\Big]. \quad (9)$$

The maximum probability density is defined as $P_{\max}$. In order to reduce the calculation of low probability density data points, the solution is computed in a subspace ($G^*$) defined as: $P_{t,Z,\alpha} > f \times P_{\max}$, where $f$ is 0.8 in this study.
Thus, the probability density weighted values are:

$$\begin{aligned} t_\mu &= \frac{\iiint_{G^*} t\, P(t,Z,\alpha)\, dt\, dZ\, d\alpha}{\iiint_{G^*} P(t,Z,\alpha)\, dt\, dZ\, d\alpha}, \\ Z_\mu &= \frac{\iiint_{G^*} Z\, P(t,Z,\alpha)\, dt\, dZ\, d\alpha}{\iiint_{G^*} P(t,Z,\alpha)\, dt\, dZ\, d\alpha}, \\ \alpha_\mu &= \frac{\iiint_{G^*} \alpha\, P(t,Z,\alpha)\, dt\, dZ\, d\alpha}{\iiint_{G^*} P(t,Z,\alpha)\, dt\, dZ\, d\alpha}. \end{aligned} \quad (10)$$

The associated errors are:

$$\begin{aligned} \sigma_t^2 &= \frac{\iiint_{G^*} (t-t_\mu)^2\, P(t,Z,\alpha)\, dt\, dZ\, d\alpha}{\iiint_{G^*} P(t,Z,\alpha)\, dt\, dZ\, d\alpha}, \\ \sigma_Z^2 &= \frac{\iiint_{G^*} (Z-Z_\mu)^2\, P(t,Z,\alpha)\, dt\, dZ\, d\alpha}{\iiint_{G^*} P(t,Z,\alpha)\, dt\, dZ\, d\alpha}, \\ \sigma_\alpha^2 &= \frac{\iiint_{G^*} (\alpha-\alpha_\mu)^2\, P(t,Z,\alpha)\, dt\, dZ\, d\alpha}{\iiint_{G^*} P(t,Z,\alpha)\, dt\, dZ\, d\alpha}. \end{aligned} \quad (11)$$

The results are summarized in Table 2.

## 4 RESULTS

### 4.1 Stellar Age and Metallicity

The stellar ages and metallicities derived by the above three different methods are presented in Table 2, and compared with each other in Figures 2 and 3. For succinct discussion, we name each parameter in the different method as follows: 'Starlight' as SL, EZ_Ages as EZ, and the probability density method as PD.

Because EZ and PD are both based on the Lick/IDS index system, and use H$\beta$ as the age indicator, the data points are equally distributed near $x = y$ in the $\mathrm{Age_{EZ}}$-$\mathrm{Age_{PD}}$ plot (Fig. 2). However, there is an aberration near the upper limit ($\sim 13-15$ Gyr), which is caused by the different maximum age definitions in the EZ and PD models: the maximum model age of EZ is 15.8 Gyr, while for PD, it is 15 Gyr (maximum model age of TMB03). In order to compare with SL (the main purpose of this paper), whose maximum model age is 13 Gyr, we also set 13 Gyr as the maximum model age of PD. Before comparing $\mathrm{Age_{SL}}$ with $\mathrm{Age_{PD}}$, the Lick indices of three EGs (NGC 3226, NGC 4278 and NGC 4486) are found to lie outside of the stellar model grids because the H$\beta$ indices are too small, which is obvious in the calculation result of EZ ("NAN"). In these galaxies, we detect distinct [OIII] and H$\beta$ emission lines in the residual spectra after removing the old stellar contribution. González (1993) suggested that such emission lines arise from ionized gas, thus the H$\beta$ indices of these three galaxies are questionable. We especially clean the emission lines of these three galaxies using the residual spectra output from 'Starlight'. These revised ages are comparable with $\mathrm{Age_{SL}}$ as shown in the plot of $\mathrm{Age_{SL}}$-$\mathrm{Age_{PD}}$. On the other hand, in most of the low-$\sigma$ galaxies ($\triangle$) $\mathrm{Age_{SL}}$ is larger than $\mathrm{Age_{PD}}$, and it is more significant

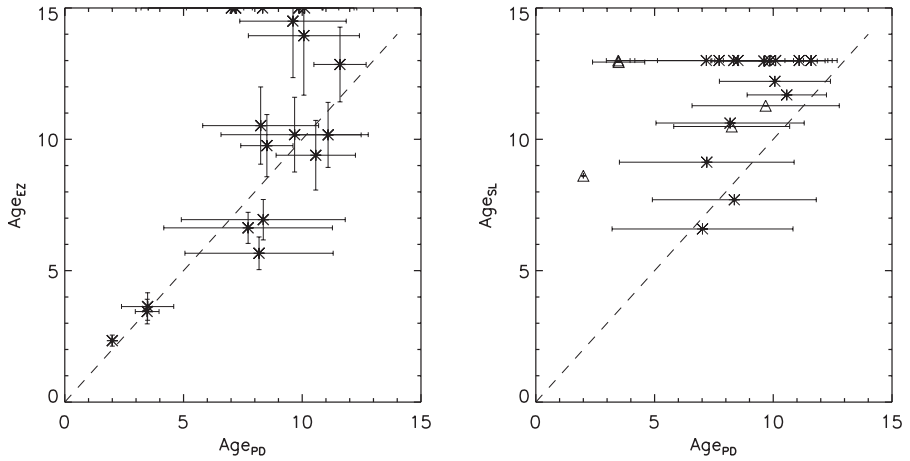


**Fig. 2** Comparison of stellar ages determined by different methods. The dashed line in each panel represents $x = y$, the symbols $\triangle$ represent inactive galaxies.

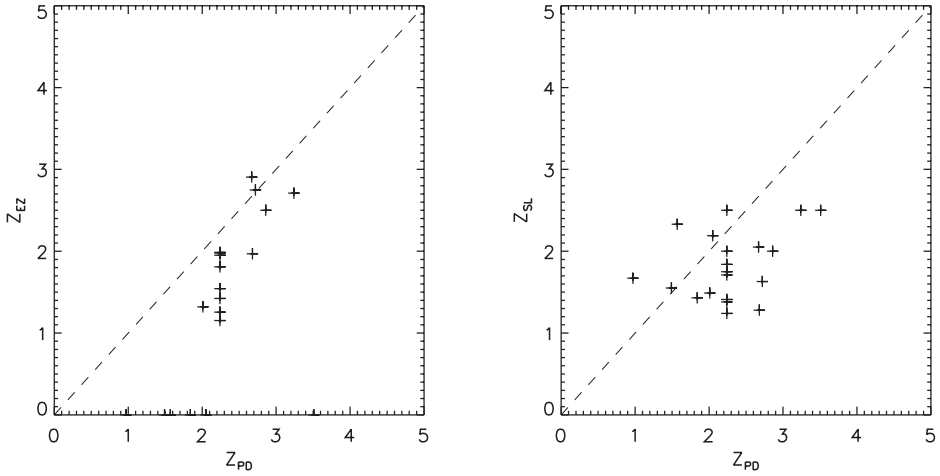


**Fig. 3** Comparison of stellar metallicities determined by different methods.

in some galaxies, such as NGC 3377, NGC 3610, and NGC 3640. Burstein et al. (1984) suggested three possible explanations for this enhanced Balmer line: anomalously hot horizontal branches, blue stragglers, and younger stellar populations. Schiavon et al. (2004) constructed a diagnostic plot using the ratio of two Balmer lines $\mathrm{H}\delta_\mathrm{F}/\mathrm{H}\beta$ to distinguish different sources for the enhanced $\mathrm{H}\beta$ line. We will discuss whether a younger stellar population should be employed to explain the enhanced $\mathrm{H}\beta$ line in Section 5.

We also compare the stellar metallicities determined by different methods, as shown in Figure 3. In the $Z_\mathrm{PD}$-$Z_\mathrm{EZ}$ plot, $Z_\mathrm{PD}$ is positively correlated with $Z_\mathrm{EZ}$, with a zeropoint offset of about $0.5\,Z_\odot$. The same problem has been addressed by Graves & Schiavon (2008), where they pointed out that $[\mathrm{Fe/H}]$ determined by EZ_Ages was 0.08 dex lower than that of TMB05. We convert it to [Z/H], which is about $0.5\,Z_\odot$. This means that $Z_\mathrm{PD}$ is consistent with TMB05, and again proves the validity of the PD program. On the other hand, in the $Z_\mathrm{PD}$-$Z_\mathrm{SL}$ plot, $Z_\mathrm{PD}$ is positively correlated with $Z_\mathrm{SL}$, with a

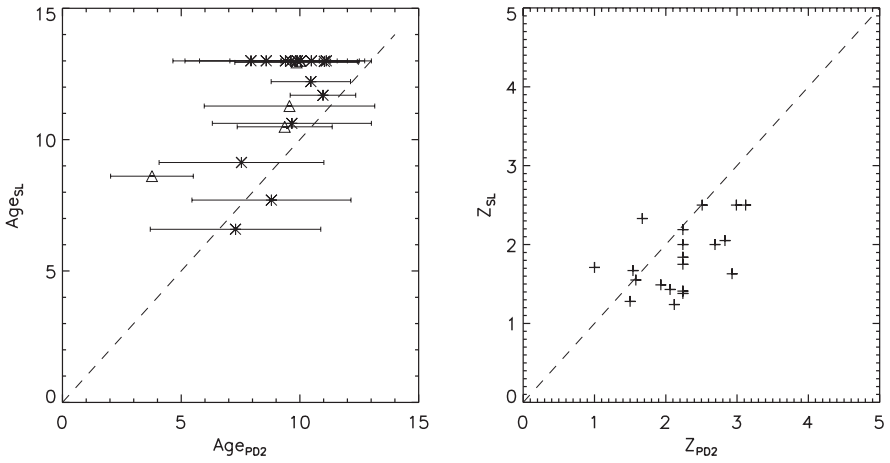


**Fig. 4** Stellar ages and metallicities determined by the probability density method using $\mathrm{H}\gamma_{\mathrm{F}}$ as an age indicator, and compared with those of 'Starlight'.

zeropoint offset of about 0.5 $Z_{\odot}$, consistent with Cid Fernandes et al. (2005). We will return to this issue and discuss it in more detail in Section 5.

We know that high-order Balmer lines, such as $\mathrm{H}\gamma$ and $\mathrm{H}\delta$, are less affected by young populations, and are more suitable age indicators for old stellar populations (Worthey 1996b; Worthey & Ottaviani 1997). We choose $(\mathrm{H}\gamma_{\mathrm{F}}, \langle\mathrm{Fe}\rangle, \mathrm{Mgb})$ as input parameters, and derive the stellar ages and metallicities of our sample by the probability density method (PD2 for short), which are shown in Figure 4. In an $\mathrm{Age_{SL}}$-$\mathrm{Age_{PD2}}$ plot, we find that, except for NGC 3610, the data points are equally distributed near $x = y$. The studies of stellar age are usually scaled in logarithm ($\log(\mathrm{Age}) \sim 6 - 10$), thus natural coordinates in the comparison of this study indicate that the accordant relation is a relatively good one. In other words, because the galaxies in our sample are mostly old, they are concentrated in the age distribution. If we add some late-type galaxies into the sample, the accordant relation will be more distinct.

### 4.2 Abundance vs. Galaxy Mass

Based on the different sensitivity of Lick indices to abundance variations (Korn et al. 2005), the Lick indices are divided into different groups. For example, Balmer lines are considered to be the indicator of stellar age. $\mathrm{H}\beta$ was widely used in the past because it was revealed to be the most sensitive age indicator (Worthey 1994); however, due to probable contamination from young stellar populations and the presence of higher quality spectra, higher-order Balmer lines (e.g. $\mathrm{H}\gamma$, $\mathrm{H}\delta$) are frequently employed nowadays. The Lick indices for metallicity are divided into two groups: the Fe-peak elements (e.g. Fe 5270, Fe 5335), which are mainly released in type Ia supernovae, and the $\alpha$ elements (e.g. $\mathrm{Mgb}$) which are produced by type II supernovae. TMB05 proposed that the ratio of $\alpha$ elements to Fe-peak elements ($[\alpha/\mathrm{Fe}]$) reflects the star formation history. A lot of work has shown that the element abundances correlate tightly with stellar velocity dispersion (stellar mass) in EGs (Kuntschner 2000; TMB05).

Figures 5–8 show the correlation of velocity dispersion to each Lick index, with the Pearson correlation coefficient in the top-right of each figure.

1. Balmer lines: A clear inverse correlation can be found in $\mathrm{H}\gamma_{\mathrm{F}}$ plot, but the case is more complicated in the $\mathrm{H}\beta$ plot. In the $\mathrm{H}\beta$ plot, two high-$\sigma$ galaxies confuse the inverse trend. Though the correlation is mild, it is obvious that the massive EGs are older.

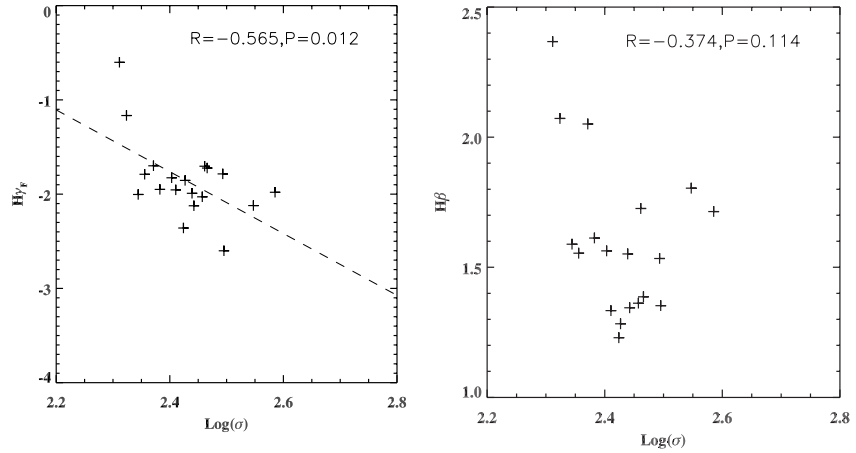


**Fig. 5** Balmer lines vs. $\log(\sigma)$, the dashed line represents the linear fitting.

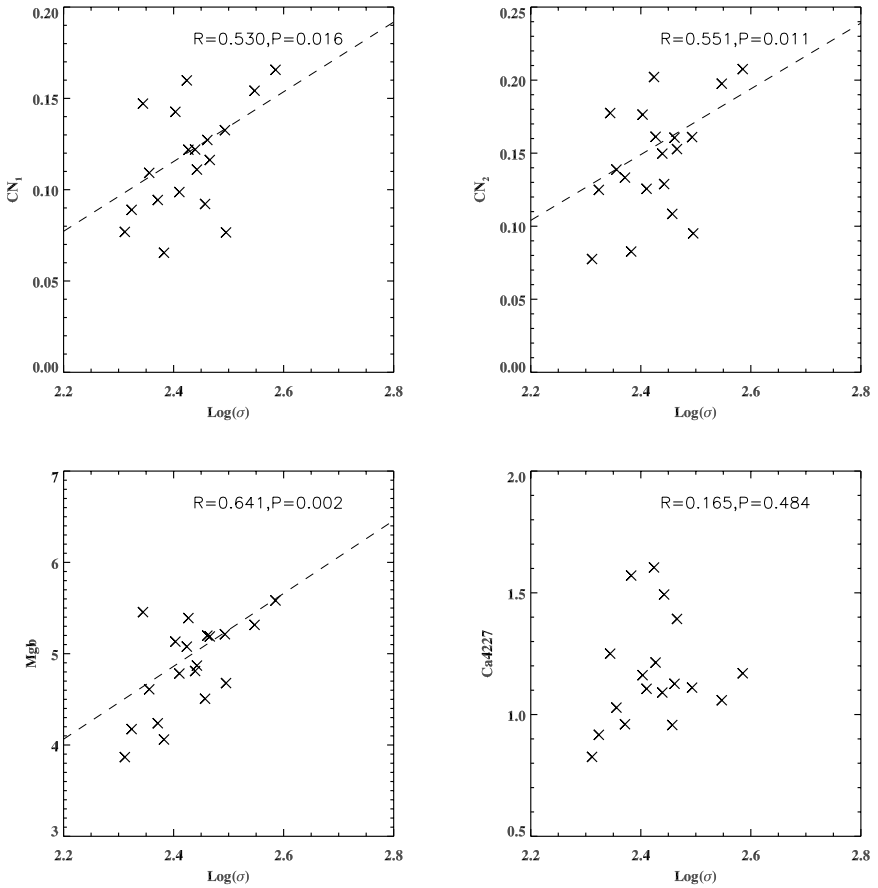


**Fig. 6** $\alpha$ elements vs. $\log(\sigma)$, the dashed line represents the linear fitting.

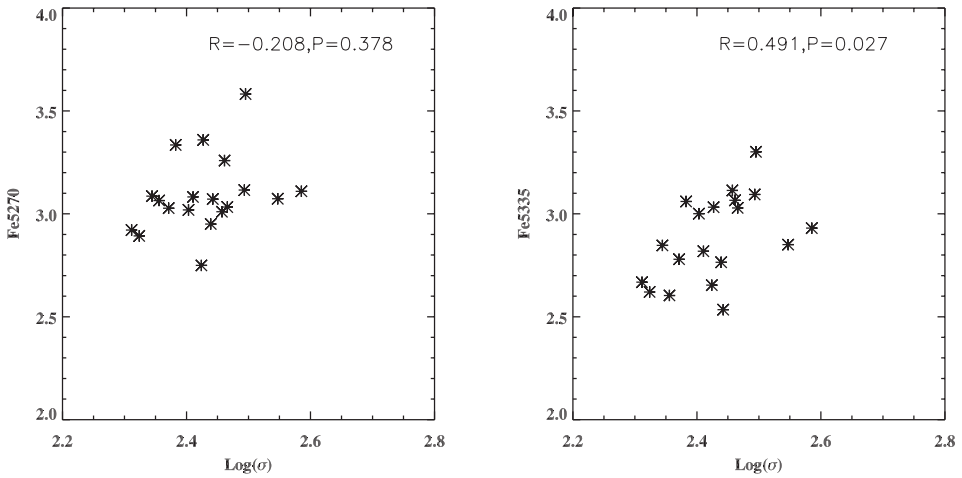


**Fig. 7** Fe-peak elements vs. $\log(\sigma)$.

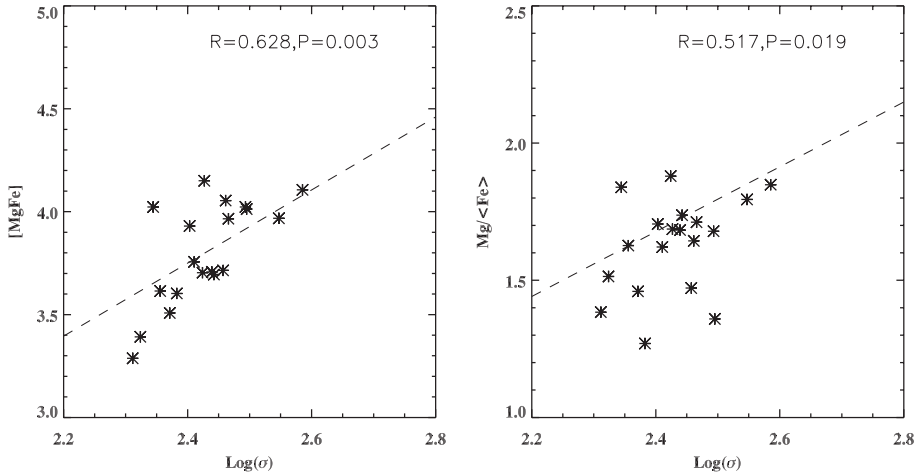


**Fig. 8** Metallicity and $\alpha$ element enhancement vs. $\log(\sigma)$. The dashed line represents the linear fitting.

2. $\alpha$ elements: In the $\mathrm{Mgb}$, $\mathrm{CN_1}$, $\mathrm{CN_2}$, and $\mathrm{Ca}$ 4227 plots, positive correlations are found, except for $\mathrm{Ca}$ 4227. Studies have found that the property of $\mathrm{Ca}$ 4227 does not resemble other $\alpha$ elements, but is more like Fe-peak elements (Trager et al. 1998; TMB03). Recently, Prochaska et al. (2005) pointed out that $\mathrm{Ca}$ 4227 is contaminated by the nearby $\mathrm{CN}$ line in the blue pseudocontinuum, and this causes the different property related to $\mathrm{Ca}$ 4227. Redefining the pseudocontinuum bandpass of $\mathrm{Ca}$ 4227 will reveal the $\alpha$ element property. The $\mathrm{Mg}$-$\sigma$ relation has been well studied (Trager et al. 2000b; Kuntschner 2000). This relation indicates that the $\alpha$ elements produced by type II supernovae are more in massive EGs. We derived the $\mathrm{Mg}$-$\sigma$ relation, which is: $\mathrm{Mgb} = -4.719 + 3.992\log(\sigma)$.
3. Fe-peak elements: For $\mathrm{Fe}$ 5270, $\mathrm{Fe}$ 5335, the correlation with velocity dispersion is not obvious. This phenomenon is also found in Worthey (1996b); Huang & Gu (2009), and the reason is still under debate.
4. Metallicity: We refer to the method in González (1993), and construct the index $[\mathrm{MgFe}] = \sqrt{\mathrm{Mgb}\cdot\langle\mathrm{Fe}\rangle}$. The $[\mathrm{MgFe}]$ index is proven to be insensitive to $[\alpha/\mathrm{Fe}]$ in TMB03. In our sample,

the $[\mathrm{MgFe}]$ plot shows the positive correlation between metallicity and galaxy mass – metallicity is richer in a massive galaxy. The relation is fitted as: $[\mathrm{MgFe}] = -0.509 + 1.775\log(\sigma)$.

5. $\alpha$ element enhancement: $\mathrm{Mg}/\langle\mathrm{Fe}\rangle$ is depicted as the indicator of star formation timescale in recent studies (TMB05). Trager et al. (2000b) found a good positive correlation of $[\alpha/\mathrm{Fe}]$-$\sigma$ after analyzing a sample of nearby galaxies. However, Kuntschner et al. (2001) found a mild $[\alpha/\mathrm{Fe}]$-$\sigma$ relation for early-type galaxies in group and cluster environments. The $\mathrm{Mg}/\langle\mathrm{Fe}\rangle$ plot in our paper also shows a mild correlation, which is fitted as: $\mathrm{Mg}/\langle\mathrm{Fe}\rangle = 1.157 + 1.181\log(\sigma)$.

## 5 DISCUSSION

### 5.1 Comparison

In this paper, we show the validity of the PD program after comparing $\mathrm{Age}_{\mathrm{EZ}}$-$\mathrm{Age}_{\mathrm{PD}}$ and $Z_{\mathrm{EZ}}$-$Z_{\mathrm{PD}}$. We note that H$\beta$ (the age indicator) is affected by several factors: (1) a few percent of the young stellar population in an old population background will significantly affect H$\beta$; (2) H$\beta$ from an ionized interstellar medium will reduce the equivalent width of the absorption line (González 1993). However, the high-order Balmer line ($\mathrm{H}\gamma_{\mathrm{F}}$) is less affected by these factors (Worthey 1996b; Worthey & Ottaviani 1997), thus stellar age and metallicity can be determined more accurately. We find that, except for NGC 3610, the data points are equally distributed near $x = y$ in the plot of $\mathrm{Age}_{\mathrm{SL}}$-$\mathrm{Age}_{\mathrm{PD2}}$. Since our sample galaxies are all ellipticals, except for three enhanced H$\beta$ line galaxies (showing young stellar populations), the stellar ages of purely old galaxies are concentrated around 10 Gyr. If we add some late-type galaxies, the accordant relation will be more distinct. On the other hand, the stellar metallicities ($Z_{\mathrm{SL}}$) are positively correlated with $Z_{\mathrm{PD2}}$ with a zeropoint offset of about 0.5 $Z_{\odot}$. Cid Fernandes (private communication) suggested that the different estimations of metallicity in the Lick method and 'Starlight' are responsible for this. 'Starlight' mixes 6 metallicities which are available in BC03, while the Lick method computes metallicity using response functions and it depends on different $\alpha/\mathrm{Fe}$ (not included in BC03). Thus, the zeropoint offset is predictable. The values computed by the empirical population synthesis method (SL) and the Lick/IDS index system method are consistent with each other for the purely old EGs.

### 5.2 Two-Component Stellar Population

The explanation for the enhanced H$\beta$ line in EGs is always a hot topic since the application of Lick indices. Burstein et al. (1984) suggested three possible explanations for this enhanced H$\beta$ line: anomalously hot horizontal branches, blue stragglers, and younger stellar populations. Though the younger stellar population model was more preferred (Burstein et al. 1984; Trager et al. 2000a; Trager et al. 2005), Maraston & Thomas (2000) showed that an enhanced H$\beta$ line can be produced by mixing old metal-rich and old metal-poor components. They hinted that an old metal-poor stellar population emits radiation in the mid-UV ($2000 - 4000$ Å), and it is thus easier to constrain a reasonable model. In order to distinguish different sources for the enhanced H$\beta$ line on the basis of optical spectra, Schiavon et al. (2004) constructed a diagnostic plot using the ratio of two Balmer lines ($\mathrm{H}\delta_{\mathrm{F}}/\mathrm{H}\beta$). The $\mathrm{H}\delta_{\mathrm{F}}/\mathrm{H}\beta$ of three enhanced H$\beta$ line galaxies in our sample (NGC 3377, NGC 3610, and NGC 3640) are relatively small (maximum value is 0.5) compared to the critical value 0.8 in figure 3 of Schiavon et al. (2004). Thus, the two-component stellar population model should be employed to explain these enhanced H$\beta$ line galaxies. Serra & Trager (2007) have studied the Lick/IDS indices of composite stellar populations, a combination of one old and one young stellar population. Note that the difference between H$\beta$- and H$\gamma$-based ages ($\mathrm{Age}_{\mathrm{H}\beta}$, $\mathrm{Age}_{\mathrm{H}\gamma}$) correlates with the mass ratio of the young to old population, and the age of the young population (fig. 3 in Serra & Trager 2007); we speculate that the mass ratio of the young to old population is larger in NGC 3610 than in NGC 3377 and NGC 3640 — $\mathrm{Age}_{\mathrm{PD}}$ and $\mathrm{Age}_{\mathrm{PD2}}$ of NGC 3610 are both too young compared to $\mathrm{Age}_{\mathrm{SL}}$. NGC 3610 is closely investigated by the *Hubble* in Whitmore et al. (1997). After studying the colors and magnitudes of the globular clusters in NGC 3610, they concluded it had a stellar age of 4 Gyr. This is consistent with $\mathrm{Age}_{\mathrm{PD2}}$ in our study, but a bit

younger compared to $\mathrm{Age_{SL}}$. Multi-wavelength images and spectral observations are needed to verify the two-component stellar population model in these low-density galaxies.

The two-component stellar population model is frequently employed to explain the observed young stellar populations, and even star-forming activity in multi-wavelengths. Kaviraj et al. (2007) and Yi et al. (2005) found recent star formation within the last 1 Gyr by the UV color-magnitude relation. In the near infrared, Silva et al. (2008) studied the K-band spectral indices, and concluded that the two-component model could explain the too-young age in the Age-$\sigma$ relation, consistent with the optical outcomes. Whether young star formation ($< 1$ Gyr) or intermediate age stars ($\sim 2-4$ Gyr) should be employed as a young population could be determined by near infrared emission lines. Hyvönen et al. (2009) asserted that massive stars passing the red giant phase will explode as supernovae, and the emission lines [FeII] (1.644 $\mu$m) and $\mathrm{H_2}$1-0 S(1) (2.212 $\mu$m) should be seen. In the radio band, Grossi et al. (2009) found that the detection rate of HI is much higher in the low-density environment than their high-density counterparts, because the HI is related to star formation. In the optical band, Rose et al. (1994) proposed that intermediate age populations exist in the low-density environment EGs. Trager et al. (2000a) proposed the "frosting" model, a double starburst model in which a small "frosting" of a young population forms upon an old population. Sánchez-Blázquez et al. (2006b, 2009) and Trager & Somerville (2009) find that low-density environment galaxies span a larger range in SSP age and metallicity than their high-density counterparts. In our study, the enhanced H$\beta$ line galaxies (NGC 3377, NGC 3610, and NGC 3640) belong to the low-density part of the whole sample. This confirms that the stellar populations in low-density environment galaxies are more diverse compared to their high-density counterparts.

### 5.3 Explanations for Abundance$-\sigma$ Relations

Many studies have tried to explain the relations between abundance and velocity dispersion (Kuntschner 2000, 2001; Trager et al. 2000b; TMB05; Sánchez-Blázquez et al. 2006b ), but a mature model still needs more time. In this study, we try to explore the effect of environment ($\sigma$) on galaxy evolution based on previous studies.

1. Balmer lines: In fact, the Balmer line-$\sigma$ relation has the same meaning as the Age-$\sigma$ relation, and it confirms that the stellar populations in low-density environment galaxies are more diverse compared to their high-density counterparts. This "down-sizing" effect suggests either that the episodes of star formation have had a larger influence on the low-density galaxies, or that the last star formation activity occurs on average later in low-density galaxies (Sánchez-Blázquez et al. 2006b). TMB05 showed that most star formation in EGs is expected to happen between redshifts $z \sim 3-5$ in high-density galaxies, and redshifts $z \sim 1-2$ in their low-density counterparts.
2. $\alpha$ element enhancement: A mild $[\alpha/\mathrm{Fe}]$-$\sigma$ relation is found in our study, as is the case in Kuntschner (2000); TMB05; Sánchez-Blázquez et al. (2006b). The mechanism behind this relation has always been a hot topic in recent studies. $\alpha$ elements are believed to be released in Type II supernovae, while at least 2/3 of Fe-peak elements are produced by Type Ia supernovae, with a delay of $\sim 1$ Gyr. Worthey et al. (1992) pointed out three possible explanations: (1) different timescales for star formation; (2) variable IMFs; and (3) selective loss mechanisms. TMB05 suggested that a different star formation timescale is the most reasonable mechanism for the $[\alpha/\mathrm{Fe}]$-$\sigma$ relation, and it could be parameterized by $[\alpha/\mathrm{Fe}]$ as (assuming $\Delta t$ is the star-forming timescale):

$$[\alpha/\mathrm{Fe}] = 1/5 - 1/6 \log \Delta t. \quad (12)$$

   To sum up, the abundance-$\sigma$ relations suggest that galaxies in low-density and high-density environments experience different formation and evolution stages.

## 6 CONCLUSIONS

In this paper, we observed high resolution spectra for a sample of 20 elliptical galaxies from Ho et al. (1997). By employing the probability density method, we determined their stellar ages and metallici-

ties. After comparing the results with different methods, we found that, though the zeropoint offset exists in stellar metallicity, the stellar ages and metallicities from the empirical population synthesis method and the Lick/IDS index system method are consistent with each other for the purely old EGs. We confirmed that the stellar populations in low-density environment galaxies are more diverse compared to their high-density counterparts.

**Acknowledgements** The authors are very grateful to the anonymous referee for his constructive report which improved the paper very much. This work is supported by the Program for New Century Excellent Talents in University (NCET), the National Natural Science Foundation of China (Grant Nos. 10878010, 10221001 and 10633040), and the National Basic Research Program (973 program No. 2007CB815405). The Starlight project is supported by the Brazilian agencies CNPq, CAPES and FAPESP and by the France-Brazil CAPES/Cofecub program. We would like to thank the staff at the Xinglong Station, the National Astronomical Observatories, CAS for their painstaking efforts during the observation.

## References

Annibali, F., Bressan, A., Rampazzo, R., Zeilinger, W. W., & Danese, L. 2007, A&A, 463, 455
Bica, E. 1988, A&A, 195, 76
Bruzual, G., & Charlot, S. 2003, MNRAS, 344,1000 (BC03)
Burstein, D., Faber, S. M., Gaskell, C. M., & Krumm, N. 1984, ApJ, 287, 586
Cardelli, J. A., Clayton, G. C., & Mathis, J. S. 1989, ApJ, 345, 245
Cardiel, N., Gorgas, J., Cenarro, J., & González, J. J. 1998, A&AS, 127, 597
Cid Fernandes, R., Sodré, L., Schmitt, H. R., & Leão, J. R. S. 2001, MNRAS, 325, 60
Cid Fernandes, R., et al. 2004, MNRAS, 355, 273
Cid Fernandes, R., Mateus, A., Sodré, L., Stasińska, G., & Gomes, J. M. 2005, MNRAS, 358, 363
Faber, S. M., Friel, E. D., Burstein, D., & Gaskell, C. M. 1985, ApJS, 57, 711
González, J. J. 1993, Ph.D. thesis, Univ. California Santa Cruz
Graves, G. J., & Schiavon, R. P. 2008, ApJS, 177, 466
Grossi, M., et al. 2009, A&A, 498, 407
Gu, Q., Melnick, J., Cid Fernandes, R., Kunth, D., Terlevich, E., & Terlevich, R. 2006, MNRAS, 366, 480
Ho, L. C., Filippenko, A. V., & Sargent, W. L. W. 1995, ApJS, 98, 477
Ho, L. C., Filippenko, A. V., & Sargent, W. L. W. 1997, ApJS, 112, 315
Huang, S., & Gu, Q. S. 2009, MNRAS, 398, 1651
Hyvönen, T., Kotilainen, J. K., Reunanen, J., & Falomo, R. 2009, 499, 417
Kaneda, H., Onaka, T., & Sakon, I. 2005, ApJ, 632, L83
Kaneda, H., et al. 2008, ApJ, 684, 270
Kaviraj, S., et al. 2007, ApJS, 173, 619
Knapp, G. R., Guhathakurta, P., Kim, D. W., & Jura, M. A. 1989, ApJS, 70, 329
Korn, A. J., Maraston, C., & Thomas, D. 2005, A&A, 438, 685
Kuntschner, H. 2000, MNRAS, 315, 184
Kuntschner, H., Lucey, J. R., Smith, R. J., Hudson, M. J., & Davies, R. L. 2001, MNRAS, 323, 615
Kuntschner, H. 2004, A&A, 426, 737
Maraston, C., & Thomas, D. 2000, ApJ, 541, 126
Prochaska, L. C., Rose, J. A., & Schiavon, R. P. 2005, AJ, 130, 2666
Rose, J. A., et al. 1994, AJ, 108, 2054
Sánchez-Blázquez, P., Gorgas, J., Cardiel, N., & González, J. J. 2006b, A&A, 457, 809
Sánchez-Blázquez, P., et al. 2009, A&A, 499, 47
Schiavon, R. P., Rose, J. A., Courteau, S., & MacArthur, L. A. 2004, ApJ, 608, L33
Schiavon, R. P. 2007, ApJS, 171, 146
Serra, P., & Trager, S. C. 2007, MNRAS, 374, 769
Serven, J., Worthey, G., & Briley, M. M. 2005, ApJ, 627, 754
Silva, D. R., Kuntschner, H., & Lyubenova, M. 2008, ApJ, 674, 194

Temi, P., Brighenti, F., Mathews, W. G., & Bregman, J. D. 2004, ApJS, 151, 237
Thomas, D., Maraston, C., & Bender, R. 2003, MNRAS, 339, 897 (TMB03)
Thomas, D., Maraston, C., Bender, R., & Mendes de Oliveira, C. 2005, ApJ, 621, 673 (TMB05)
Trager, S. C., Worthey, G., Faber, S. M., Burstein, D., & González, J. J. 1998, ApJS, 116,1
Trager, S. C., Faber, S. M., Worthey, G., & González, J. J. 2000a, AJ, 119, 1645
Trager, S. C., Faber, S. M., Worthey, G., & González, J. J. 2000b, AJ, 120, 165
Trager, S. C., Worthey, G., Faber, S. M., & Dressler, A. 2005, MNRAS, 362, 2
Trager, S. C., & Somerville, R. S. 2009, MNRAS, 395, 608
Whitmore, B. C., Miller, B. W., Schweizer, F., & Fall, S. M. 1997, AJ, 114, 1797
Worthey, G., Faber, S. M., & González, J. J. 1992, ApJ, 398, 69
Worthey, G. 1994, ApJS, 95, 107
Worthey, G. 1996a, in IAU Symp. 171, New Light on Galaxy Evolution, eds. R. Bender, & R. L. Davies (Kluwer Academic Publisher), 71
Worthey, G. 1996b, in ASP Conf Ser., 98, From Stars to Galaxies: The Impact of Stellar Physics on Galaxy Evolution, eds. C. Leitherer, U. Fritze-von Alvensleben, & J. Huchra (San Francisco: ASP), 467
Worthey, G., & Ottaviani, D. L. 1997, ApJS, 111, 377
Yi, S. K., et al. 2005, ApJ, 619, L111
Zorotovic, M., et al. 2009, AJ, 137, 257